Vol 442|6 July 2006|doi:10.1038/nature04857 nature

LETTERS

Resonance in the electron-doped high-transition-temperature superconductor $Pr_{0.88}LaCe_{0.12}CuO_{4-\delta}$

Stephen D. Wilson[1], Pengcheng Dai[1,2], Shiliang Li[1], Songxue Chi[1], H. J. Kang[3,4] & J. W. Lynn[3]

In conventional superconductors, the interaction that pairs the electrons to form the superconducting state is mediated by lattice vibrations[1] (phonons). In high-transition-temperature (high-T_c) copper oxides, it is generally believed that magnetic excitations might play a fundamental role in the superconducting mechanism because superconductivity occurs when mobile 'electrons' or 'holes' are doped into the antiferromagnetic parent compounds[2]. Indeed, a sharp magnetic excitation termed 'resonance' has been observed by neutron scattering in a number of hole-doped materials[3–11]. The resonance is intimately related to superconductivity[12], and its interaction with charged quasi-particles observed by photoemission[13,14], optical conductivity[15], and tunnelling[16] suggests that it might play a part similar to that of phonons in conventional superconductors. The relevance of the resonance to high-T_c superconductivity, however, has been in doubt because so far it has been found only in hole-doped materials[17]. Here we report the discovery of the resonance in electron-doped superconducting $Pr_{0.88}LaCe_{0.12}CuO_{4-\delta}$ (T_c = 24 K). We find that the resonance energy (E_r) is proportional to T_c via $E_r \approx 5.8k_BT_c$ for all high-T_c superconductors irrespective of electron- or hole-doping. Our results demonstrate that the resonance is a fundamental property of the superconducting copper oxides and therefore must be essential in the mechanism of superconductivity.

Although the interaction of electrons with phonons or magnetic excitations can cause electron pairing and superconductivity, we focus on magnetic excitations because the resonance is intimately related to superconductivity and is also present in several classes of hole-doped high-T_c materials. The resonance is a sharp magnetic excitation centred at the wavevector $\mathbf{Q} = (1/2, 1/2)$ in the two-dimensional reciprocal space of the CuO_2 planes, which corresponds to the antiferromagnetic Bragg position of the undoped compounds (Fig. 1a). It was first discovered in the hole-doped bilayer (each lattice unit cell has two CuO_2 planes) high-T_c superconductor $YBa_2Cu_3O_{6+x}$ (YBCO)[3]. Its intensity grows below T_c and its energy ($\hbar\omega$) scales approximately with k_BT_c (Fig. 1e)[4–8]. At energies below the resonance, spin fluctuations peak at incommensurate wavevectors[8] and disperse inwards towards the resonance[18,19]. Such behaviour is remarkably similar to that of the hole-doped $La_{2-x}(Ba,Sr)_xCuO_4$ (refs 20–22). Although the resonance has also been observed in the hole-doped bilayer $Bi_2Sr_2CaCu_2O_{8+\delta}$ (called Bi(2212))[9,10] and in the single-layer $Tl_2Ba_2CuO_{6+\delta}$[11], the wavevector and energy dependence of the mode has been determined only for YBCO[3–8] because of the small available single crystal volumes in the Bi(2212)[9,10] and $Tl_2Ba_2CuO_{6+\delta}$[11]. Therefore, it has not been possible directly and systematically to compare the neutron results with those of the photoemission, which are obtained mostly for Bi(2212)[13,14].

Here we studied the magnetic excitations of electron-doped materials to understand the electron–hole symmetry in high-T_c superconductors. We grew large single crystals of $Pr_{0.88}LaCe_{0.12}CuO_{4-\delta}$ (PLCCO) using the travelling solvent floating zone technique and annealed the samples to obtain optimal superconductivity with T_c = 24 K (Fig. 1a)[23,24]. PLCCO is a single-layer electron-doped copper oxide and was chosen to avoid the static antiferromagnetic order that coexists with superconductivity in $Nd_{1.85}Ce_{0.15}CuO_4$ (NCCO)[25]; the T_c = 24 K PLCCO is phase pure, without static antiferromagnetic order[23,26]. Our elastic $\mathbf{Q}$-scans through the expected antiferromagnetic Bragg positions confirmed no static antiferromagnetic order to at least 600 mK in our PLCCO samples (Figs 1b and 1c).

We first probed the low-energy magnetic excitations of PLCCO using the Spin-Polarized Inelastic Neutron-Scattering Spectrometer (SPINS). The magnetic excitations were commensurate and centred around $\mathbf{Q} = (1/2,1/2,0)$ at all temperatures (Figs 2a–c), similar to those of NCCO[25]. They can be well described by gaussians on linear backgrounds and are not resolution-limited. Fourier transforms of the gaussian peaks in Figs 2a–c gave dynamic spin correlation lengths of $\xi \approx 96 \pm 15$, 80 ± 10 and 94 ± 24 Å for $\hbar\omega$ = 0.5, 1.5 and 3.5 meV, respectively. With increasing temperature, the scattering above background was virtually unchanged from 2 K ($T_c - 22$ K) to 30 K ($T_c + 6$ K) but decreased slightly at 55 K owing to increased background (Figs 2a–c). The temperature dependence of the scattering at $\hbar\omega$ = 1.5 meV showed no observable anomaly across T_c (Fig. 2d), thus suggesting that the magnetic excitations are gapless and different from those of NCCO[25]. The energy scans at $\mathbf{Q} = (1/2, 1/2, 0)$ confirmed that the magnetic scattering between 0.5 and 4.5 meV is virtually temperature independent between 2 and 30 K (Fig. 2e), and therefore does not follow the population factor $1/(1 - e^{-\hbar\omega/k_BT})$ expected for simple bosonic excitations.

To study the magnetic excitations for energies above 4.5 meV, we used the HB-1 and BT-9 thermal neutron triple-axis spectrometers. Figure 3a–c shows $\mathbf{Q}$-scans through (1/2, 1/2, 0) for $\hbar\omega$ = 3.5, 8.0 and 10 meV at T = 2, 30 and 80 K. In contrast to the temperature-independent low-energy ($\hbar\omega \leq 4.5$ meV) magnetic excitations below T_c (Fig. 2), the integrated intensity above background around (1/2, 1/2, 0) at $\hbar\omega$ = 8 and 10 meV shows a significant enhancement on cooling from 30 K to 2 K, but hardly changes on warming from 30 K to 80 K (Fig. 3b and c). The $\mathbf{Q}$-width of the peak at $\hbar\omega$ = 10 meV is temperature-independent and resolution-limited, giving a minimum $\xi \approx 45 \pm 5$ Å (Fig. 3c). Similar scans using better collimations on BT-9 (Fig. 4e) are again resolution-limited, giving $\xi \approx 51 \pm 7$ Å. Figure 3d shows energy scans at the peak centre [$\mathbf{Q} = (1/2, 1/2, 0)$] compared to background [$\mathbf{Q} = (0.5875, 0.5875, 0)$] positions for temperatures 2, 30 and 80 K. The weak, dispersion-less peak at $\hbar\omega$ = 6 meV and the gradual rising background scattering with increasing energy are due to the Pr^{3+} crystalline electric-field excitations in the tetragonal unit cell of PLCCO[27]. Its intensity simply

[1]Department of Physics and Astronomy, The University of Tennessee, Knoxville, Tennessee 37996-1200, USA. [2]Center for Neutron Scattering, Oak Ridge National Laboratory, Oak Ridge, Tennessee 37831, USA. [3]NIST Center for Neutron Research, National Institute of Standards and Technology, Gaithersburg, Maryland 20899-8562, USA. [4]Department of Materials Science and Engineering, University of Maryland, College Park, Maryland 20742, USA.

produces a shift in the background scattering on which the sharply localized magnetic excitations at $\mathbf{Q} = (1/2,\ 1/2,\ 0)$ rest (see Supplementary Information). The temperature difference spectrum (2 K–30 K) shows a clear intensity gain around ~11 meV at $\mathbf{Q} = (1/2,\ 1/2,\ 0)$ (Fig. 3e).

Figure 4a shows the energy dependence of the scattering at $\mathbf{Q} = (1/2,\ 1/2,\ 0)$ and background (0.6, 0.6, 0) positions using BT-9. The scattering at (1/2, 1/2, 0) around ~11 meV is systematically higher below T_c while the background intensity at (0.6, 0.6, 0) is temperature-independent between 2 K and 30 K. The temperature difference spectrum below and above T_c (2 K–30 K) in Fig. 4c shows a clear resolution-limited resonance peak centred at $\hbar\omega \approx 11$ meV, consistent with Fig. 3e. A constant energy scan at $\hbar\omega = 10$ meV confirms that the peak is centred at (1/2, 1/2, 0) (Fig. 4b) while a similar scan at $\hbar\omega = 15$ meV shows only background scattering (Fig. 4b). Finally, in Fig. 4d we plot the temperature dependence of the scattering at (1/2, 1/2, 0) and the integrated intensity around (1/2, 1/2, 0) above the background for $\hbar\omega = 10$ meV. They both increase dramatically below the onset of T_c and are remarkably similar to that of the optimally doped YBCO[3,4] and Bi(2212)[9].

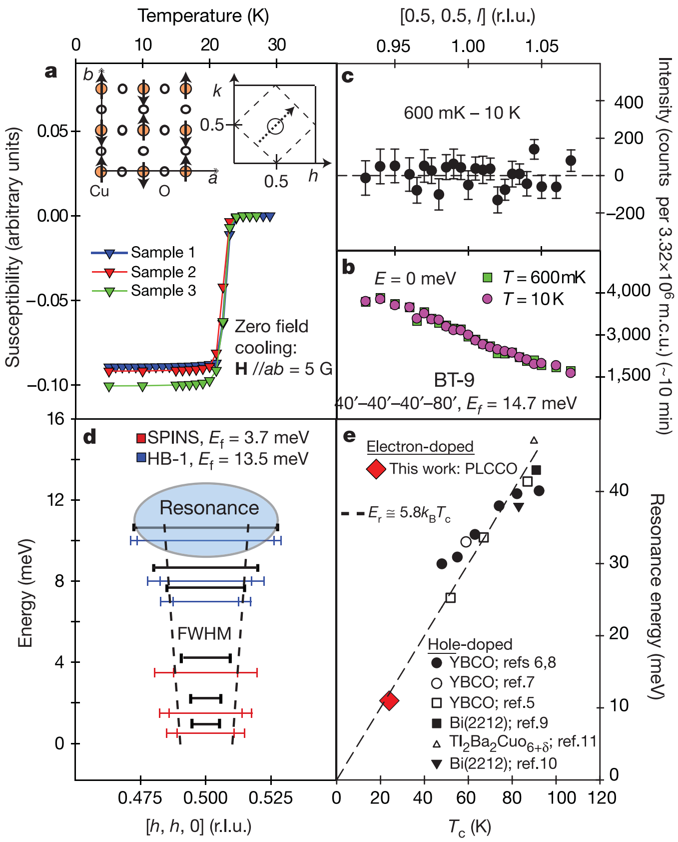

Figure 1 | Magnetic susceptibility and a summary of neutron-scattering results. a, Schematic diagrams of real and reciprocal space of the CuO_2 with the dashed box showing the first Brillouin zone and the dotted arrow indicating the Q-scan direction. The temperature dependence of the magnetic susceptibility for the three crystals (mosaicity < 1°) was investigated. Our neutron-scattering experiments were performed using pyrolytic graphite for monochromators and analysers on the HB-1 triple-axis spectrometer at the High-Flux Isotope Reactor, Oak Ridge National Laboratory, and on the SPINS and BT-9 triple-axis spectrometers at the NIST Center for Neutron Research. We label the momentum transfer $\mathbf{Q} = (q_x, q_y, q_z)$ as $(h, k, l) = (q_x a/2\pi,\ q_y a/2\pi,\ q_z c/2\pi)$ in the reciprocal lattice units (r.l.u.) appropriate for the tetragonal unit cell of PLCCO ($a = b = 3.98$, and $c = 12.27$ Å). The three single crystals, with a total mass of ~9 g, are co-aligned to within 1° in the $[h, h, l]$ or $[h, k, 0]$ zones. **b**, Elastic scattering along the [0.5, 0.5, l] direction through the (0.5, 0.5, 1) antiferromagnetic Bragg position at 600 mK and 10 K (ref. 23). The temperature difference spectrum in **c** shows no static antiferromagnetic order at 600 mK. In all figures, the vertical error bars are statistical uncertainties (1σ) assuming a Poisson distribution function as defined in intensity-type measurements. **d**, The full-width at half-maximum (FWHM) of the magnetic response with the instrumental resolution marked as horizontal bars. The dashed lines are guides to the eye. **e**, Summary of the resonance energy as a function of T_c for hole-doped YBCO (refs 3–8), Bi(2212) (refs 9, 10), $Tl_2Ba_2CuO_{6+\delta}$ (ref. 11), and electron-doped PLCCO (this work). The dashed line is the best fit with $E_r = 5.8\ k_B T_c$. It takes about 10 min to run the specified monitor count units (m.c.u.).

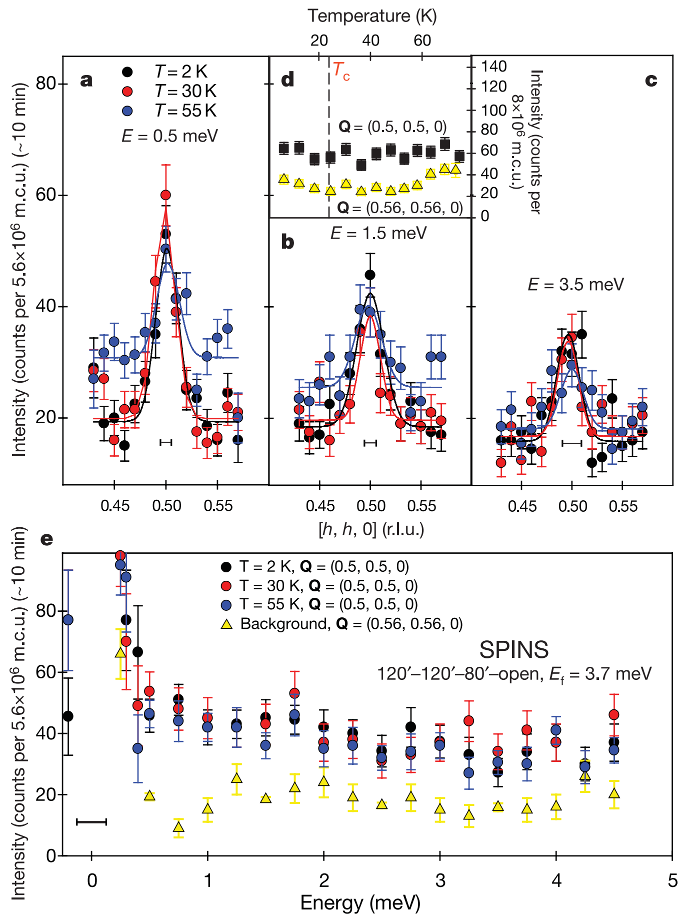

Figure 2 | The wavevector, energy and temperature dependence of the magnetic scattering around $\mathbf{Q} = (1/2, 1/2, 0)$ for $0.5 \le \hbar\omega \le 4.5$ meV. The experiments were performed on SPINS with a fixed neutron final energy $E_f = 3.7$ meV and a cold Be filter before the analyser. Error bars are 1σ. **a–c**, Q-scans along the $[h, h, 0]$ direction for $\hbar\omega = 0.5$, 1.5 and 3.5 meV at $T = 2$, 30, and 55 K. Centred brackets (in all figures) indicate instrumental resolutions. For $\hbar\omega = 0.5$ meV, gaussian fits on linear backgrounds give an amplitude $A = 31.3 \pm 4.2$ counts per 10 min, width $W = 0.011 \pm 0.0016$ r.l.u., background $= 19.2 \pm 1.2$ counts per 10 min at 2 K; $A = 38.3 \pm 4.9$ counts per 10 min, $W = 0.0104 \pm 0.0014$ r.l.u., background $= 19.9 \pm 1.2$ counts per 10 min at 30 K. For $\hbar\omega = 3.5$ meV, $A = 19.9 \pm 5.2$ counts per 10 min, $W = 0.0098 \pm 0.0027$ r.l.u., background $= 16.1 \pm 1.3$ counts per 10 min at 2 K; $A = 16.6 \pm 4.9$ counts per 10 min, $W = 0.0094 \pm 0.0029$ r.l.u., background $= 16.9 \pm 1.2$ counts per 10 min at 30 K. At $\hbar\omega = 0.5$ meV, the integrated intensities (defined as the sum of raw scanned intensities above the linear fitted background) are 96 ± 15 counts per 10 min at 2 K and 105 ± 14 counts per 10 min at 30 K. At $\hbar\omega = 3.5$ meV, they are 61 ± 12 counts per 10 min at 2 K and 61 ± 12 counts per 10 min at 30 K. **d**, Temperature-dependent scattering at $\mathbf{Q} = (1/2, 1/2, 0)$ and (0.56, 0.56, 0) for $\hbar\omega = 1.5$ meV. The background is independent of temperature below ~50 K and the magnetic signal becomes much weaker at 80 K. **e**, Constant-Q scans obtained on SPINS with spectrometer collimations as shown, at the ridge of magnetic scattering at 2, 30 and 55 K, compared with the temperature-independent background scattering for $2 \le T \le 30$ K.

To summarize the neutron scattering results in Figs 2–4, we plotted the dispersion of the observed magnetic excitations in Fig. 1d and the resonance energy as a function of T_c in Fig. 1e (refs 3–12). Although the magnetic excitations are broader than the instrumental resolution for $\hbar\omega \leq 3.5$ meV and resolution-limited for $\hbar\omega \geq 4.5$ meV, they are commensurate and centred at (1/2, 1/2, 0) at all measured energies. This differs from the hole-doped materials, where incommensurate spin fluctuations below the resonance merge into it[18–21]. On the other hand, the resonance energy of 11 meV ($E_r \approx 5.3k_BT_c$) for the PLCCO is remarkably close to the universal value of $E_r \cong 5.8k_BT_c$ for all materials (Fig. 1e)[3–12].

Our results reveal several important conclusions for the electron–hole symmetry of the magnetic excitations in high-T_c copper oxides. First, the discovery of the magnetic resonance in electron-doped PLCCO with $E_r \approx 5.3k_BT_c$ suggests that the resonance is a common feature for high-T_c superconductors irrespective of electron- or hole-doping. Second, the observation of commensurate spin fluctuations below the resonance (Fig. 1d) implies that the intimate connection between incommensurate spin fluctuations and the resonance in hole-doped materials is not a universal feature[18–21]. At present, it is unclear how stripe models can account for these differences[20,28]. Third, the magnetic excitations ($0.5 \leq \hbar\omega \leq 16$ meV) in the electron-doped PLCCO are gapless, decrease monotonically with increasing

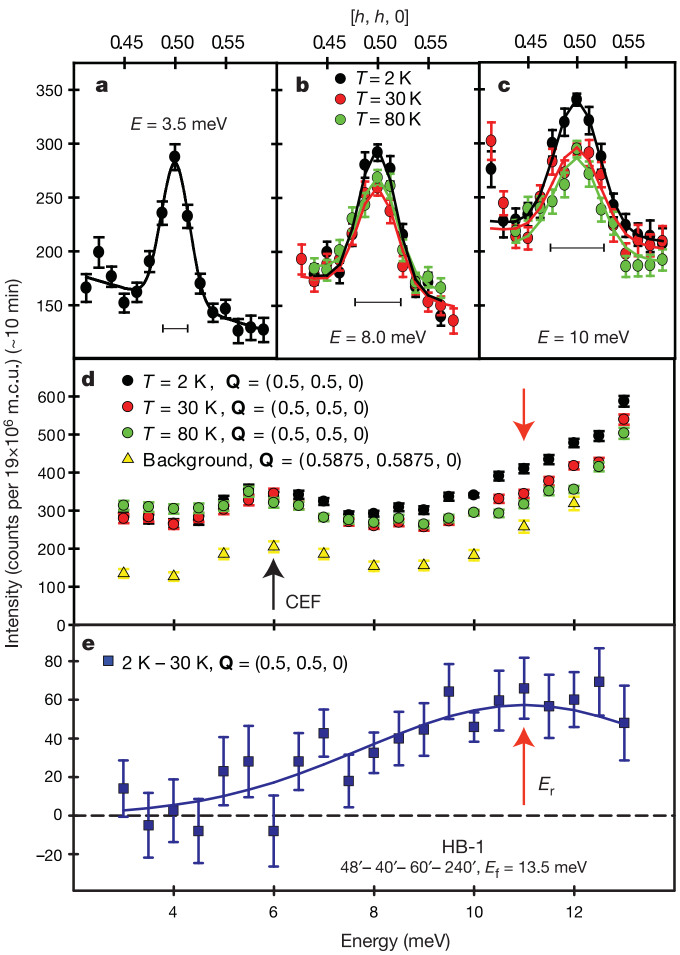

Figure 3 | The wavevector and energy dependence of the scattering around Q = (1/2, 1/2, 0) below and above T_c. The experiments were carried out on HB-1 with $E_f = 13.5$ meV and a pyrolytic graphite filter before the analyser. Error bars are 1σ. **a–c**, Q-scans along the $[h, h, 0]$ direction for $\hbar\omega = 3.5$, 8 and 10 meV at $T = 2$, 30 and 80 K. The gradual rise in the background scattering with increasing energy (and decreasing scattering angle) is due to the tail of the strong Pr^{3+} crystalline electric-field excitation at 18 meV and the low-angle background scattering[27]. For $\hbar\omega = 10$ meV, gaussian fits on sloped linear backgrounds give amplitudes $A = 122 \pm 4$ counts per 10 min, width $W = 0.023 \pm 0.001$ r.l.u., background $= 218 \pm 9$ counts per 10 min at 2 K; $A = 84 \pm 9$ counts per 10 min, $W = 0.024 \pm 0.004$ r.l.u., background $= 212 \pm 7$ counts per 10 min at 30 K; and $A = 87 \pm 9$ counts per 10 min, $W = 0.023 \pm 0.004$ r.l.u., background $= 200 \pm 7$ counts per 10 min at 80 K. **d**, Energy scans at Q = (1/2, 1/2, 0) where the magnetic scattering peaks, and background scattering at (0.587, 0.587, 0). The maximum energy transfer of 13 meV at Q = (1/2, 1/2, 0) is limited by kinematic constraints. The weak dispersionless peak at 6 meV arises from a previously unknown Pr^{3+} crystalline electric-field (CEF) level. Its intensity is temperature-independent between 2 and 30 K within the statistics of our measurements and thus can be regarded as background scattering. **e**, The temperature difference spectrum between 2 and 30 K suggests a resonance-like enhancement at ~11 meV. See the Supplementary Information for more details on the temperature dependence of the crystalline electric-field levels.

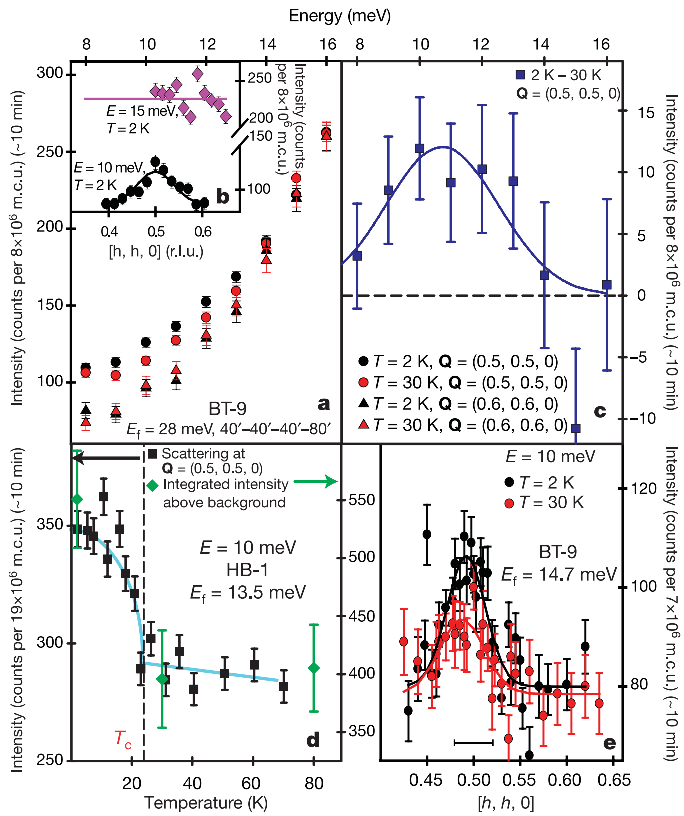

Figure 4 | The wavevector, energy and temperature dependence of the scattering around Q = (1/2, 1/2, 0). Data in **a–c** are collected using BT-9 with $E_f = 28$ meV and a pyrolytic graphite filter before the analyser. This geometry allows the kinematic constraints to be satisfied at (1/2, 1/2, 0) for $\hbar\omega \leq 16$ meV. Error bars are 1σ. **a**, The energy scans along the ridge of magnetic scattering at (1/2, 1/2, 0) were counted for ~2 h per point to obtain the statistics shown. The background scattering at (0.6, 0.6, 0) was counted for ~30 min per point and showed no observable difference between 2 K and 30 K. **b**, Wavevector scans along the $[h, h, 0]$ direction around (1/2, 1/2, 0) at $\hbar\omega = 10$ and 15 meV. The kinematic constraints allow only half of the Q-scan at $\hbar\omega = 15$ meV. **c**, Temperature difference (2 K–30 K) spectrum at Q = (1/2, 1/2, 0) shows the resolution-limited resonance at $\hbar\omega = 11$ meV. The energy resolution of the spectrometer is ~3.7 meV in FWHM at $\hbar\omega = 10$ meV. **d**, Black squares show temperature dependence of the neutron intensity (~1 h per point) at (1/2, 1/2, 0) and 10 meV obtained on HB-1 (Fig. 3). Green diamonds are integrated intensity of the localized signal centred around Q = (1/2, 1/2, 0) above background in Fig. 3c. The line is a guide to the eye. **e**, Q-scans at $\hbar\omega = 10$ meV obtained on BT-9 with $E_f = 14.7$ meV and collimations 40′-40′-40′-80′. The gaussian fits have $A = 25.4 \pm 3.4$ counts per 10 min, $W = 0.022 \pm 0.004$ r.l.u., background $= 80 \pm 3$ counts per 10 min at 2 K and $A = 15.2 \pm 2.7$ counts per 10 min, $W = 0.023 \pm 0.005$ r.l.u., background $= 78 \pm 2$ counts per 10 min at 30 K.

energy, and are virtually temperature-independent between $2\,K \le T \le 30\,K$ except for the appearance of the resonance below T_c (Figs 2–4). Such behaviour does differ from optimally hole-doped YBCO[3–6] and $La_{2-x}Sr_xCuO_4$ (ref. 21), but the temperature-independent low-energy ($0.5\,meV \le \hbar\omega \le 4.5\,meV$) magnetic scattering is remarkably similar to the quantum critical scattering in heavy fermion $UCu_{5-x}Pd_x$ (ref. 29). Finally, the discovery of the magnetic resonance in electron-doped PLCCO, in which charged quasiparticles can also be probed by photoemission[30], allows a systematic comparison of their properties in the same bulk sample, which has not hitherto been possible for any other high-T_c superconductors. This should open new avenues of research aiming to understand the exotic properties of high-T_c copper oxides.

Received 9 February; accepted 27 April 2006.

1. Bardeen, J., Cooper, L. N. & Schrieffer, J. R. Theory of superconductivity. *Phys. Rev.* **108,** 1175–1204 (1957).
2. Orenstein, J. & Millis, A. J. Advances in the physics of high-temperature superconductivity. *Science* **288,** 468–474 (2000).
3. Rossat-Mignod, J. *et al.* Neutron scattering study of the $YBa_2Cu_3O_{6+x}$ system. *Physica C* **185,** 86–92 (1991).
4. Mook, H. A. *et al.* Polarized neutron determination of the magnetic excitations in $YBa_2Cu_3O_7$. *Phys. Rev. Lett.* **70,** 3490–3493 (1993).
5. Fong, H. F. *et al.* Spin susceptibility in underdoped $YBa_2Cu_3O_{6+x}$. *Phys. Rev. B* **61,** 14773–14786 (2000).
6. Dai, P., Mook, H. A., Hunt, R. D. & Doğan, F. Evolution of the resonance and incommensurate spin fluctuations in superconducting $YBa_2Cu_3O_{6+x}$. *Phys. Rev. B* **63,** 054525 (2001).
7. Stock, C. *et al.* Dynamic stripes and resonance in the superconducting and normal phases of $YBa_2Cu_3O_{6.5}$ ortho-II superconductor. *Phys. Rev. B* **69,** 014502 (2004).
8. Hayden, S. M., Mook, H. A., Dai, P., Perring, T. G. & Doğan, F. The structure of the high-energy spin excitations in a high-transition-temperature superconductor. *Nature* **429,** 531–534 (2004).
9. Fong, H. F. *et al.* Neutron scattering from magnetic excitations in $Bi_2Sr_2CaCu_2O_{8+\delta}$. *Nature* **398,** 588–591 (1999).
10. He, H. *et al.* Resonant spin excitations in a overdoped high temperature superconductor. *Phys. Rev. Lett.* **86,** 1610–1613 (2001).
11. He, H. *et al.* Magnetic resonant mode in the single-layer high-temperature superconductor $Tl_2Ba_2CuO_{6+\delta}$. *Science* **295,** 1045–1047 (2002).
12. Dai, P. *et al.* The magnetic excitation spectrum and thermodynamics of high-T_c superconductors. *Science* **284,** 1344–1347 (1999).
13. Damascelli, A., Hussain, Z. & Shen, Z.-X. Angle-resolved photoemission studies of the cuprate superconductors. *Rev. Mod. Phys.* **75,** 473–541 (2003).
14. Norman, M. R. & Pepin, C. The electron nature of high temperature cuprate superconductors. *Rep. Prog. Phys.* **66,** 1547–1610 (2003).
15. Basov, D. N. & Timusk, T. Electrodynamics of high-T_c superconductors. *Rev. Mod. Phys.* **77,** 721–779 (2005).
16. Zasadzinski, J. F. *et al.* Correlation of tunneling spectra in $Bi_2Sr_2CaCu_2O_{8+\delta}$ with the resonance spin excitation. *Phys. Rev. Lett.* **87,** 067005 (2001).
17. Hwang, J., Timusk, T. & Gu, G. D. High-transition-temperature superconductivity in the absence of the mangetic-resonance mode. *Nature* **427,** 714–717 (2004).
18. Arai, M. *et al.* Incommensurate spin dynamics of underdoped superconductor $YBa_2Cu_3O_{6.7}$. *Phys. Rev. Lett.* **83,** 608–611 (1999).
19. Bourges, P. *et al.* The spin excitation spectrum in superconducting $YBa_2Cu_3O_{6.85}$. *Science* **288,** 1234–1237 (2000).
20. Tranquada, J. M. *et al.* Quantum magnetic excitations from stripes in copper oxide superconductors. *Nature* **429,** 534–538 (2004).
21. Christensen, N. B. *et al.* Dispersive excitations in the high-temperature superconductor $La_{2-x}Sr_xCuO_4$. *Phys. Rev. Lett.* **93,** 147002 (2004).
22. Tranquada, J. M. Neutron scattering studies of antiferromagnetic correlations in cuprates. Preprint at ⟨http://arXiv.org/cond-mat/0512115⟩ (2005).
23. Dai, P. *et al.* Electronic inhomogeneity and competing phases in electron-doped superconducting $Pr_{0.88}LaCe_{0.12}CuO_{4-\delta}$. *Phys. Rev. B* **71,** 100502(R) (2005).
24. Kang, H. J. *et al.* Electronically competing phases and their magnetic field dependence in electron-doped nonsuperconducting and superconducting $Pr_{0.88}LaCe_{0.12}CuO_{4-\delta}$. *Phys. Rev. B* **71,** 214512 (2005).
25. Yamada, K. *et al.* Commensurate spin dynamics in the superconducting state of an electron-doped cuprate superconductor. *Phys. Rev. Lett.* **90,** 137004 (2003).
26. Fujita, M. *et al.* Magnetic and superconducting phase diagram of electron-doped $Pr_{1-x}LaCe_xCuO_4$. *Phys. Rev. B* **67,** 014514 (2003).
27. Boothroyd, A. T., Doyle, S. M., Paul, McK. D. & Osborn, R. Crystal-field excitations in Nd_2CuO_4, Pr_2CuO_4, and related *n*-type superconductors. *Phys. Rev. B* **45,** 10075–10086 (1992).
28. Kivelson, S. A. *et al.* How to detect fluctuating stripes in the high-temperature superconductors. *Rev. Mod. Phys.* **75,** 1201–1241 (2003).
29. Aronson, M. C. *et al.* Non-Fermi-liquid scaling of the magnetic response in $UCu_{5-x}Pd_x$ ($x = 1, 1.5$). *Phys. Rev. Lett.* **75,** 725–728 (1995).
30. Matsui, H. *et al.* Direct observation of a nonmonotonic $d_{x^2-y^2}$-wave superconducting gap in the electron-doped high-T_c superconductor $Pr_{0.89}LaCe_{0.11}CuO_4$. *Phys. Rev. Lett.* **95,** 017003 (2005).

Supplementary Information is linked to the online version of the paper at www.nature.com/nature.

Acknowledgements We thank E. Dagotto, H. Ding and S. Zhang for discussions. We also thank Y. Ando's group for teaching us how to grow high-quality single crystals of PLCCO. S.D.W. and S.L. are supported by the US National Science Foundation. S.C. is supported by the US DOE Division of Materials Science, Basic Energy Sciences. Oak Ridge National Laboratory is supported by the US DOE through UT/Battelle LLC. SPINS is supported by the US National Science Foundation through the Center for High Resolution Neutron Spectroscopy.

Author Information Reprints and permissions information is available at npg.nature.com/reprintsandpermissions. The authors declare no competing financial interests. Correspondence and requests for materials should be addressed to P.D. (daip@ornl.gov).